Theor Appl Climatol (2013) 112:351–361
DOI 10.1007/s00704-012-0739-2

ORIGINAL PAPER

Estimation of urban heat island intensity using biases in surface air temperature simulated by a nonhydrostatic regional climate model

Akihiko Murata · Hidetaka Sasaki · Mizuki Hanafusa · Kazuo Kurihara

Received: 5 April 2012 / Accepted: 25 July 2012 / Published online: 8 August 2012

Abstract This study demonstrates that urban heat island (UHI) intensity can be estimated by comparing observational data and the outputs of a well-developed high-resolution regional climate model. Such an estimate is possible because the observations include the effects of UHI, whereas the model used does not include urban effects. Therefore, the errors in the simulated surface air temperature, defined as the difference between simulated and observed temperatures (simulated minus observed), are negative in urban areas but 0 in rural areas. UHI intensity is estimated by calculating the difference in temperature error between urban and rural areas. Our results indicate that overall UHI intensity in Japan is 1.5 K and that the intensity is greater in nighttime than in daytime, consistent with the previous studies. This study also shows that root mean square error and the magnitude of systematic error for the annual mean temperature are small (within 1.0 K).

1 Introduction

Extensive efforts have been made to investigate future climate projections. Projections of future temperature are important both for the health of humans and ecosystems and for various industries, such as agricultural and energy industries. General circulation models (GCMs) have been used in many studies to project future temperatures. Recently, interest in projecting future temperatures on regional and local scales using regional climate models (RCMs) has been stimulated by the ability to capture spatially and temporally finer-scale temperature (e.g., Kurihara et al. 2005; Rummukainen 2010; Arritt and Rummukainen 2011).

It is necessary to validate temperature in the present-day climate using simulation by an RCM before projecting temperature in future climates in order to evaluate the reliability of the model's performance. Several studies have focused on evaluating temperature in the present-day climate simulated by RCMs. For example, Zhu and Liang (2007) used an RCM with a horizontal grid spacing of 30 km and evaluated its capability to simulate interannual variations of surface air temperature over USA. This study demonstrated that the model has a pronounced downscaling skill for interannual variations of temperature. Kostopoulou et al. (2009) assessed the accuracy of maximum and minimum temperature data from an RCM with a 25-km horizontal resolution, across the Balkan Peninsula. The model was generally accurate in describing the seasonal cycle as well as simulating the spatial distribution of temperature. Urrutia and Vuille (2009) demonstrated that an RCM with a horizontal grid spacing of 50 km adequately simulated the spatial and temporal variability of temperature in the tropical Andes, although some systematic errors (biases) were observed.

The spatial resolution of previous RCMs was not fine enough to resolve regional-scale and local-scale temperatures, especially involving interactions with complex topography. Recently, high-resolution RCMs developed from nonhydrostatic mesoscale models have been used to simulate regional climates in Japan (e.g., Sasaki et al. 2008; Kanada et al. 2008; Murata et al. 2012; Nakano et al. 2012). For example, Murata et al. (2012) demonstrated that root mean square errors (RMSEs) in daily mean and minimum temperatures reproduced by an RCM were smaller than those reproduced by the driving GCM with a coarser spatial resolution, although differences in biases of daily temperatures between RCM and GCM were not statistically significant.

A. Murata (✉) · H. Sasaki · M. Hanafusa · K. Kurihara
Meteorological Research Institute,
Tsukuba, Ibaraki 305-0052, Japan
e-mail: amurata@mri-jma.go.jp

These studies, however, used results obtained from model simulations with a limited period each year (from June to October). Sasaki et al. (2011), therefore, conducted high-resolution regional climate simulations for all seasons of each year (from January to December) and reported on the overall performance of a well-developed, high-resolution nonhydrostatic RCM (NHRCM). In this study, we used the data obtained from NHRCM simulations to perform detailed assessment of regional- and local-scale surface air temperatures in the present-day climate.

One factor that influences local-scale temperature is the urban heat island (UHI) phenomena. Numerous studies have focused on UHI, and many articles have discussed it (e.g., Arnfield 2003; Oke 2006; Kanda 2007; Kusaka 2008; Fujibe 2011). UHI phenomena have been detected by comparing observations in an urban area to those in surrounding rural areas. These observations are crucial not only for the understanding of urban climates, but also for improving numerical modeling of the urban atmosphere (e.g., Grimmond 2006). The effects of urbanization have also been investigated in experimental studies (e.g., Kanda 2006) and modeling studies (e.g., Masson 2006).

A basic problem with analysis of the effects of UHI is that some ambiguity remains in the division of urban and rural areas, depending on the data used (e.g., population data and satellite data). Kalnay and Cai (2003) estimated the impact of land use changes on surface warming using the difference in trends of surface air temperature between observational data and global reanalysis data, which was insensitive to surface observations.

Here, we use NHRCM output for the present-day climate simulation, instead of reanalysis data, to examine the effects of UHI. The influences of UHI must be detectable in the NHRCM output by considering that these influences were detected in reanalysis data. With this motivation in mind, we demonstrate that NHRCM actually captures signals of urbanization using errors in surface air temperature (i.e., difference between model and observed temperature).

The advantages of the current method in comparison with the previous approaches, such as those of Kalnay and Cai (2003), are shown below: (a) As mentioned above, unlike in the conventional methods, the current approach can avoid the ambiguity of the UHI definition associated with the division of urban and rural areas. (b) The fine mesh (i.e., 5 km) we used can distinguish urban and rural areas more accurately compared with coarser-mesh reanalysis data in which some urban areas are smaller than the area of one grid. (c) No urban effect has been included in the present-day climate simulation data we used, whereas reanalysis data are influenced by urban effects because a reanalysis procedure uses observations, including those in urban areas. The disadvantage of the current method is also shown below: There is an ambiguity related to the numerical setting of land surface parameterization. Nevertheless, the current results related to the UHI intensity are not significantly influenced because no effect regarding urbanization is included in land cover classification. To our knowledge, the effects of urbanization in Japan have not been investigated by comparing model outputs and observations. This technique enables evaluating UHI effects on surface air temperature for an individual urban area and for all areas in Japan as a whole.

In this study, we first evaluate the performance of NHRCM in terms of surface air temperature in the present-day climate in Japan. Next, we estimate the effects of UHI in Japan by comparing the model results and observations. The primary purpose of this study is to validate surface air temperature in the present-day climate reproduced by NHRCM against observations. More important purposes of this study are to examine the influences of urbanization on surface air temperature and to estimate the intensity of UHI in Japan from a statistical point of view.

The remainder of this paper is structured as follows. "Section 2" presents the data and the methods for numerical simulation using NHRCM. "Section 3" evaluates the performance of NHRCM with respect to surface air temperature in the present-day climate and investigates the relationship between errors in temperature and degree of urbanization. "Section 4" discusses UHI intensity in Japan, detected by comparing the temperature error and urbanization rate. Diurnal temperature range (DTR) is also discussed in association with UHI intensity. Finally, "Section 5" summarizes the main results of this study.

2 Data and methodology

The NHRCM developed by Sasaki et al. (2008) is a climate extension of the Japan Meteorological Agency Nonhydrostatic Model (JMA-NHM) (Saito et al. 2006, 2007). JMA-NHM is one of the numerical weather prediction models employed operationally at JMA. The model has fully compressible equations with a map factor and uses a semi-implicit time integration scheme. It includes the bulk-type cloud microphysics introduced by Ikawa et al. (1991). The scheme is based on Lin et al. (1983), Murakami (1990), and Murakami et al. (1994). The Kain–Fritsch convection scheme (Kain and Fritsch 1990; Kain 2004; Kato et al. 2010) is included as a cumulus scheme. For a planetary boundary layer scheme, the Mellor–Yamada–Nakanishi–Niino Level 3 scheme (Nakanishi and Niino 2004) is employed. For radiation, a clear-sky radiation scheme (Yabu et al. 2005) and a cloud radiation scheme (Kitagawa 2000) are used. The land surface scheme by Hirai and Ohizumi (2004), improved from the simple biosphere (SiB) model, is included. Land cover classification is derived from the

Global Land Cover Characterization for the SiB model from the US Geological Survey land use classification. The land cover map does not include urban areas. Bare soil or broadleaf shrubs with bare soil are assigned to urban areas. Surface air temperature (1.5-m height) is diagnosed from the surface skin temperature and the temperature of the lowest atmospheric layer, based on the Monin–Obukhov similarity theory (Beljaars and Holtslag 1991).

For long-term climate simulation, NHRCM includes a spectral boundary coupling scheme (Kida et al. 1991; Sasaki et al. 2000). In this scheme, large-scale components produced by the outer model are merged into smaller-scale components in the inner model. Consequently, no contradiction in the large-scale components exists between the inner and outer models, thereby enabling us to integrate the inner model steadily for a long period.

NHRCM has been used successfully to simulate regional climates. For example, using NHRCM with a 4-km grid spacing, Sasaki et al. (2008) conducted a 5-year integration with the analyzed boundary conditions and demonstrated that the model had the ability to reproduce temperature and precipitation in the present-day climate. Sasaki et al. (2011), using NHRCM with a 5-km grid spacing, performed a 20-year integration with predicted boundary conditions and demonstrated that the annual mean surface air temperature and precipitation in the present-day climate were reproduced well. They also confirmed that snow depth was adequately reproduced, although the values were underestimated in some areas.

The data obtained from Sasaki et al. (2011) are utilized in this study. The grid nesting strategy for numerical simulations is as follows (Fig. 1). The model domain (211×661 grid points) of NHRCM with a grid spacing of 5 km (NHRCM5) is set to cover Japan. Boundary conditions for NHRCM5 are derived from a simulation using NHRCM with a grid spacing of 15 km (NHRCM15) and a domain (229×217 grid points) that covers East Asia. The vertical coordinate of NHRCM is terrain-following and contains 40 levels, with the lowest level located 20 m from the ground surface and the highest level located at 21.9 km. Boundary conditions for NHRCM15 are derived from a simulation using an atmospheric general circulation model with a 20-km horizontal resolution (MRI-AGCM3.2S, hereafter referred to as the AGCM20) (Mizuta et al. 2012). Since AGCM20 does not contain mixing ratios of cloud condensate and precipitating hydrometeors, NHRCM15 is nested between NHRCM5 and AGCM20 to provide the mixing ratio to the lateral boundary for NHRCM5.

The AGCM20 was jointly developed by JMA and the Meteorological Research Institute of Japan and is based on a numerical weather prediction model used operationally by JMA, with several modifications in terms of radiation and land surface processes for use in climate simulations. The simulations are performed at a triangular truncation of 959 (TL959) in the horizontal direction, corresponding to a spatial resolution of 20 km (1,920×960 transform grids). The model has 60 layers in the vertical direction (top at 0.1 hPa). AGCM20 was run under the condition given by the Atmospheric Model Intercomparison Project AGCM simulation for the twentieth-century experiment of the Intergovernmental Panel on Climate Change Fourth Assessment Report (AR4) (IPCC 2007). In the simulation, monthly mean data from the Hadley Centre sea ice and sea surface temperature (SST) dataset version 1 (Rayner et al. 2003) were used for the observed SST and sea ice concentration

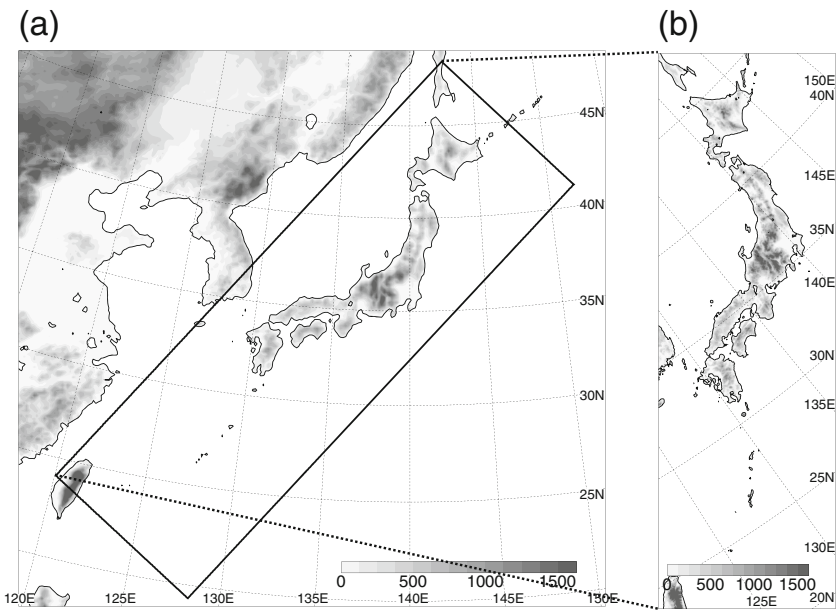

Fig. 1 Map of **a** coarse-mesh (NHRCM15) and **b** fine-mesh (NHRCM5) domains. Terrain is denoted by *shading* (m)

data. The monthly climatology of sea ice thickness from Bourke and Garrett (1987) was also used.

Simulations for the present-day climate were run for 20 years, from September 1980 to August 2000. NHRCM was initialized in August of each year and was run through August of the following year, excluding the first month of the simulation, which was discarded as model spin-up. This period of the run was selected so that the output from the model could be compared with high-spatial resolution observed meteorological data available for this period.

In this study, we report on only the model results for surface air temperature, which is considered to significantly influence the ecosystem, economy, and society. The performance of NHRCM5 was evaluated by comparing the results of the present-day climate simulation with observational data for the same period. High-resolution observations are desirable for assessing the NHRCM5 performance because of its finer grid spacing. For this purpose, we employed surface observational data with a high spatial resolution, provided by the automated meteorological data acquisition system (AMeDAS) administered by JMA. AMeDAS is a ground-based observation system and has a dense network of meteorological stations throughout Japan at an average interval of 17 km. Surface air temperature data are available at 700 of these stations. The temporal resolution (1 h) of AMeDAS data is equal to that of the NHRCM output.

3 Results

3.1 Root mean square error and systematic error in annual mean surface air temperature

Model performance in reproducing the annual mean surface air temperature in the present-day climate is assessed by comparing the NHRCM5 simulation results with observational data for the same period. As mentioned above, AMeDAS data, provided by JMA, are employed for the observed temperature data. For each AMeDAS station, data satisfying the following criteria are used: 0 % missing data over a day and less than 50 % missing data (ten data) for each calendar day over 20 years. Extraction of the model data is based on selecting the nearest land grid point to the location of each AMeDAS station. It should be noted that for each station location, there is a height discrepancy between the model and actual topographies: the elevations employed in the simulations at the station sites are generally higher than the actual elevations. Since this difference in elevation contributes to a discrepancy in temperature between the simulations and the observations, the simulated temperature is corrected using a lapse rate of 0.0065 $\mathrm{K\,m^{-1}}$. The sensitivity to lapse rate, which was stepped from 0.0060 to 0.0070 $\mathrm{K\,m^{-1}}$ in increments of 0.0005 $\mathrm{K\,m^{-1}}$, was assessed. The results were found to be insensitive to lapse rate.

RMSE and bias are calculated using the NHRCM5 simulation results and AMeDAS data in order to estimate errors in the simulated annual mean surface air temperature. Simulated data corresponding to station locations are used. RMSE and bias are defined as follows:

$$RMSE = \sqrt{\frac{1}{N}\sum_{k=1}^{N}(M_k - O_k)^2} \tag{1}$$

$$bias = \frac{1}{N}\sum_{k=1}^{N}(M_k - O_k), \tag{2}$$

where M represents simulated values, O is observations, and N ($\approx Y \times S$) is the number of data points, where Y (=20) is the number of years and S (≈700, depending on year) is the number of observing stations for which data are available. The variables selected for the calculations are the annual means of daily mean temperature (Ta), daily maximum temperature (Tx), and daily minimum temperature (Tn), where a day is defined based on local standard time (Japan Standard Time). These variables are obtained from hourly data.

RMSE and the magnitude of bias for the annual mean Ta are within 1.0 K (Fig. 2), indicating that NHRCM5 reproduces the temperature in the present-day climate well. These results suggest that NHRCM with a higher spatial resolution has the ability to capture temperature variability produced by small-scale phenomena, such as those influenced by complex topography. The magnitude of bias for the annual mean Tn is comparable to that for the annual mean Ta, whereas RMSE is somewhat larger (1.0 K). In contrast, RMSE and the magnitude of bias for the annual mean Tx are relatively large (1.5 K). The magnitude of bias is noticeable compared with those for Ta and Tn. Thus, a question arises as to why the errors in Tx are larger than those in Ta and Tn.

The horizontal distributions of errors in the annual mean Ta, Tx, and Tn are plotted in order to find reasons for the relatively large magnitude of bias in the annual mean Tx (Fig. 3). Error is defined as the difference between simulated and observed temperatures (simulated minus observed). For many areas, errors in the annual mean Tx are negative, and those in the annual mean Tn are positive (Fig. 3b, c). This result indicates that the annual mean Tx (Tn) tends to be underestimated (overestimated), consistent with the biases in Fig. 2. The magnitudes of errors in the annual mean Ta are generally smaller than those for Tx and Tn (Fig. 3a).

Negative error in the horizontal distribution of the error in the annual mean Tn is noticeable in three major metropolitan areas: Tokyo, Osaka, and Nagoya (Fig. 3c). These areas are also identified in the horizontal distribution of the error

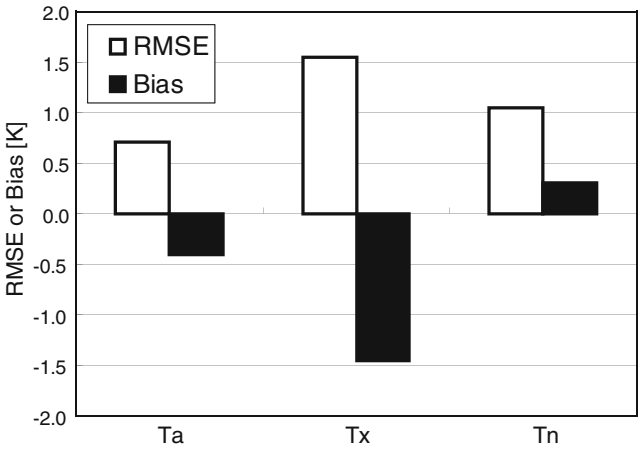

Fig. 2 Root mean square error and bias in the annual average of daily temperatures: daily mean temperature (Ta), daily maximum temperature (Tx), and daily minimum temperature (Tn) in the present-day climate reproduced by NHRCM5

in the annual mean Ta (Fig. 3a), although they are difficult to find in Tx, where the error is negative over most of Japan (Fig. 3b). The negative errors around Tokyo are consistent with Sasaki et al. (2008).

3.2 Relationship between temperature error and urbanization rate

The relationship between underestimated temperature and degree of urbanization is examined quantitatively. We used National Land Numerical Information (land utilization tertiary mesh data) provided by the Ministry of Land, Infrastructure, Transport, and Tourism to quantify the degree of urbanization. This dataset is compiled on the surface area of usage classifications in the tertiary mesh unit (1-km mesh), based on the status of nationwide land usage. Datasets for 1976, 1987, 1991, 1997, and 2006 are available.

To estimate the degree of urbanization, the urbanization rate is defined as the sum of three areas (land for building, trunk transportation land, and other land) divided by the total area (1 km^2). The urbanization rate was calculated for the 5 years indicated above; then, the results were linearly interpolated in time from 1980 to 2000 annually, during

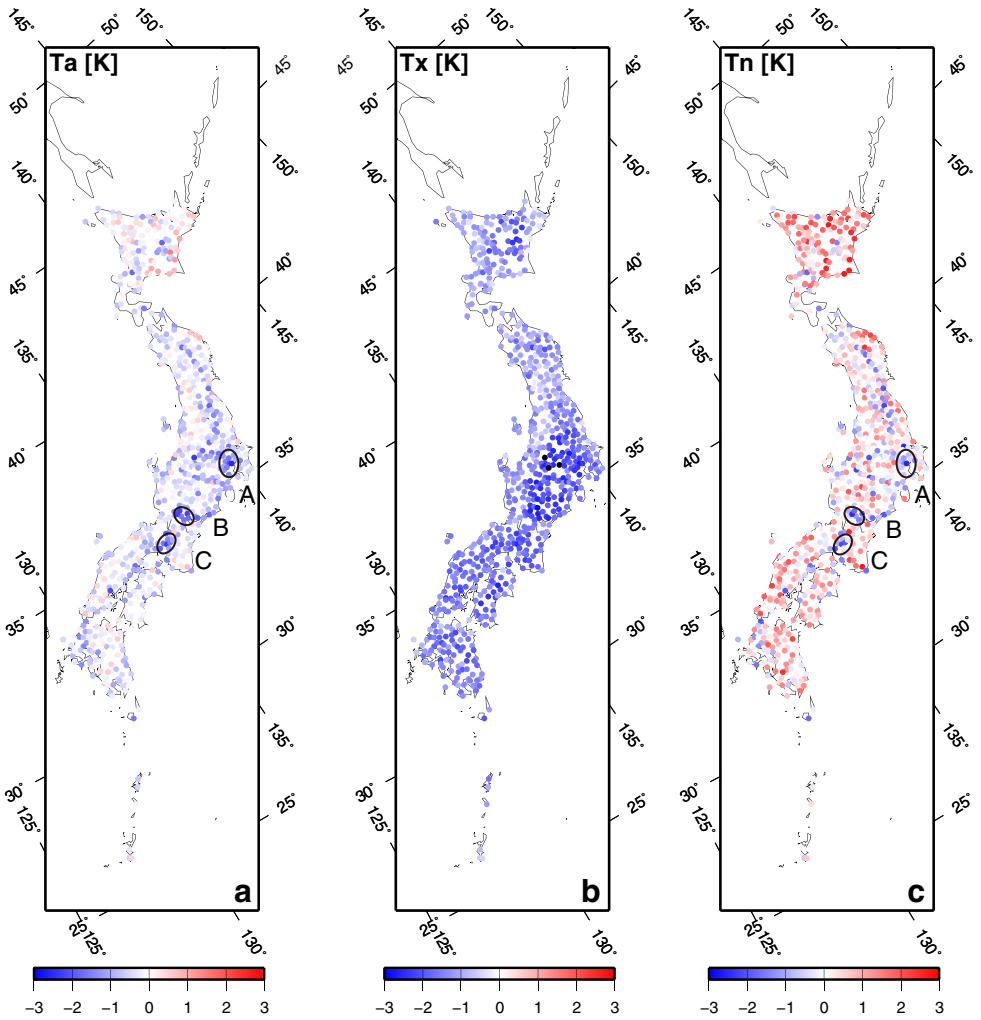

Fig. 3 Horizontal distribution of the difference in the annual average of daily temperatures: **a** daily mean temperature (Ta), **b** daily maximum temperature (Tx), and **c** daily minimum temperature (Tn) between the NHRCM5 output and the AMeDAS observation (model minus observed). Areas *A*, *B*, and *C* shown in **a** and **c** denote areas around Tokyo, Nagoya, and Osaka, respectively, where the values are negative

which NHRCM was integrated. The urbanization rate for each AMeDAS station was estimated by averaging the rate within 1 km from the station.

Scatterplots of the urbanization rate and the error in annual mean Ta, Tx, and Tn are presented in Fig. 4. The errors in Ta are small in rural areas: many data are between −1.0 K and 1.0 K when the urbanization rate is near 0. The annual mean Tx (Tn) is underestimated (overestimated) in rural areas; for the most part, the error in Tx (Tn) ranges from −2.0 K (0.0 K) to 0.0 K (2.0 K) centered at −1.0 K (1.0 K) when the urbanization rate is near 0. These results indicate that the DTR simulated by NHRCM5 is underestimated with a bias of 2 K.

In urban areas, however, annual mean temperatures are generally underestimated. The temperature errors for the three components (Ta, Tx, and Tn) are all −1.5 K when the urbanization rate is near unity (Fig. 4), at least partly because the effects of urbanization (e.g., waste heat and artificial features such as buildings and roads.) are not included in NHRCM5.

A key factor explaining why errors in the annual mean Tx exceed those in Ta and Tn is the difference in the distribution of the errors, depending on the three components. For Tn, negative errors in urban areas cancel several parts of the positive errors in rural areas (Fig. 4c), reducing positive bias and making the bias close to 0 (Fig. 2). In contrast, Tx errors are negative for all areas, although the magnitude is slightly larger in urban areas (Fig. 4b). The bias is therefore negative, and its magnitude is relatively large compared with that in Tn (Fig. 2). The bias in Ta has a value between those in Tx and Tn, consistent with the results of Tx and Tn (Fig. 4a).

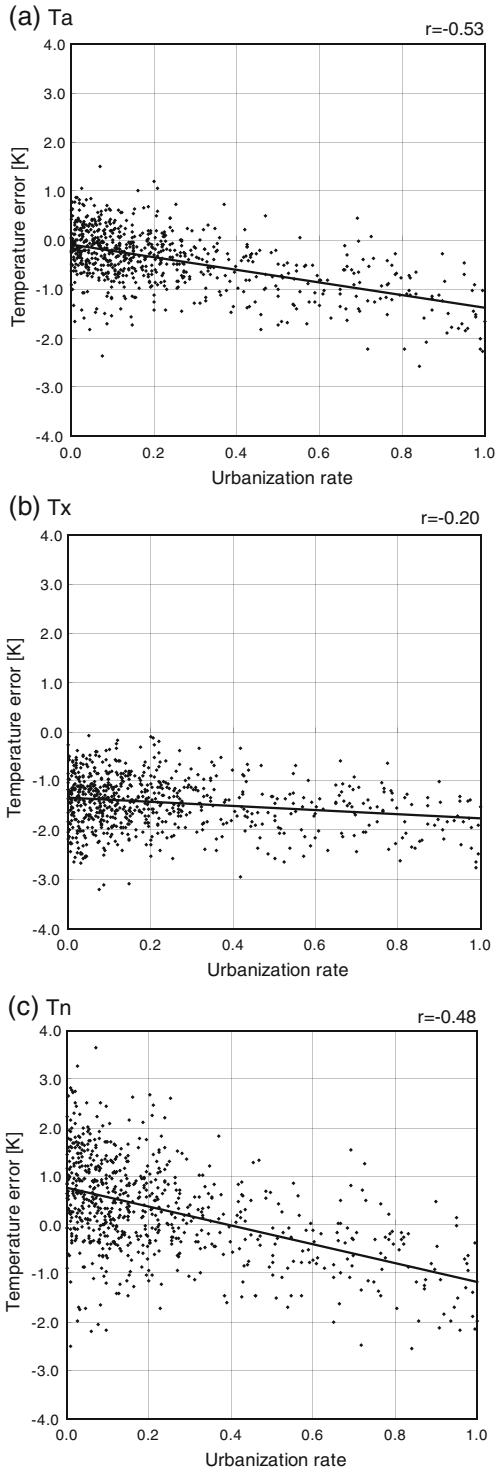

Fig. 4 Scatter diagram of urbanization rate, defined in the text, and temperature error. Differences in the annual average of daily temperatures between NHRCM5 output and AMeDAS observation (model minus observed): **a** daily mean temperature (Ta), **b** daily maximum temperature (Tx), and **c** daily minimum temperature (Tn). The *regression line* and the correlation coefficient (r) between urbanization rate and temperature error are also presented

4 Discussion

4.1 Urban heat island intensity

UHI intensity can be estimated from Fig. 4 because the effects of urbanization are evident, as mentioned in the preceding section. UHI intensity is usually defined as the difference in surface air temperature between an urban area and surrounding rural areas. In Fig. 4, the difference in temperature can be detected from a statistical point of view, although UHI intensity for each urban area cannot be evaluated. An index to evaluate statistical-viewpoint UHI intensity is defined as follows:

$$\Delta\delta T \equiv \delta T(R_u = 0.0) - \delta T(R_u = 1.0), \quad (3)$$

where δT is the error in surface air temperature (for Ta, Tx, or Tn), determined from the regression line, and R_u is the urbanization rate. For example, $\Delta\delta T$ for Ta is 1.3 K because $\delta T(R_u = 0.0)$ is −0.1 K and $\delta T(R_u = 1.0)$ is −1.4 K, considering values of δT at the intersections of the regression line and two vertical lines (R_u=0.0 and 1.0).

The index $\Delta\delta T$ for Tn is relatively large compared with that for Tx, indicating that UHI intensity is more easily detected in nighttime than in daytime. Figure 4 indicates that the index for Tx is 0.5 K and that for Tn is 2.0 K. For Ta, the index lies between those for Tx and Tn. These results are consistent with previous studies where UHI intensity is generally stronger in nighttime than in daytime (e.g., Landsberg 1981; Oke 1987). Fujibe (2011) pointed out that UHI in Japanese cities was more conspicuous in nighttime than in daytime due to low mixing depth in the stable nocturnal surface layer. Since urban environments reduce nighttime cooling and increase minimum temperature, urban areas have a lower DTR than rural areas (e.g., Kalnay and Cai 2003; Brown and DeGaetano 2010; Wang et al. 2012). DTR in the present results is examined in detail in the following subsection.

The index $\Delta\delta T$ is generally larger in winter than in summer, indicating that UHI intensity is relatively strong during the cold seasons. Figure 5 presents scatterplots of the urbanization rate and the error in the monthly mean Ta in January (corresponding to winter in Japan), April (corresponding to spring in Japan), July (corresponding to summer in Japan), and October (corresponding to fall in Japan). The index $\Delta\delta T$ can be estimated to be 1.5 K for January, 1.1 K for April, 1.2 K for July, and 1.4 K for October. These results are consistent with those of previous studies where UHI intensity is generally stronger in winter than in summer in Japan (e.g., Sakakibara et al. 1996).

It should be noted that there exist a scatter of the data in Figs. 4 and 5. Possible reasons for the scatter of the data could include the limitations of the land surface scheme and the radiation scheme. The scatter seems to be larger in daily minimum temperature than in daily maximum temperature (Fig. 4) and larger in winter than in summer (Fig. 5). These errors in lower temperature can be caused by processes associated with freezing and melting of water in the surface soil layer. In addition, the infrared radiation budget at the surface may be responsible for the errors because cloud cover, which is an important factor that contributes to the budget, has ambiguities. The results also suggest that these schemes should be more sophisticated in order to reproduce surface air temperature more accurately.

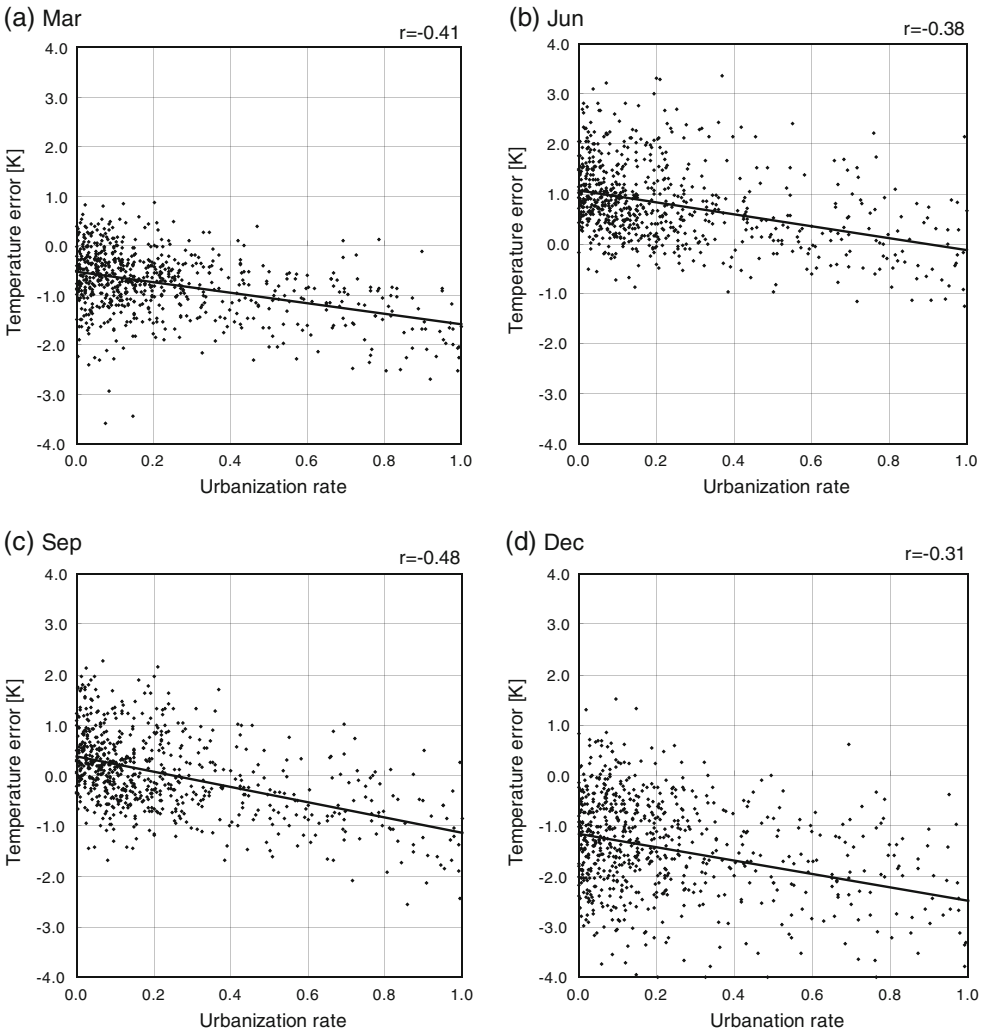

Fig. 5 Scatter diagram of urbanization rate, defined in the text, and temperature error. Difference (K) in the monthly average of daily mean temperature between NHRCM5 output and AMeDAS observation (model minus observed) in **a** March, **b** June, **c** September, and **d** December. The *regression line* and the correlation coefficient (r) between urbanization rate and temperature error are also indicated

The results presented in this subsection demonstrate that UHI intensity over an area can be estimated by comparing the model results and observational data. The model results are not influenced by UHI effects because the effects of urbanization (e.g., waste heat and artificial structures) are not included in the model. The observational data, however, are directly affected by UHI. This difference is the key factor for detecting the effects of UHI. It should be emphasized that the estimated UHI intensity is a kind of "bulk parameter," and the value can be interpreted as UHI intensity averaged over all of Japan. This kind of UHI intensity is unique because previous studies focused on UHI intensity for an individual urban area.

4.2 Diurnal temperature range

The magnitude of error in DTR is apparently smaller in urban areas than in rural areas. Figure 6a depicts a scatterplot of urbanization rate and error in the annual mean DTR. The errors are −2.0 K when the urbanization rate is near 0.0, and −0.5 K when the urbanization rate is near 1.0. The apparent reduction in magnitude of error is mainly due to the fact that the observed DTR actually has smaller values in urban areas than in rural areas. In Fig. 6b, the observed annual mean DTR is 9.0 K when the urbanization rate is near 0.0, and it is 8.0 K when the urbanization rate is near 1.0. The difference in the observed DTR (1.0 K) can account for most of the difference in DTR error (1.5 K) between the urban and rural areas. However, the simulated annual mean DTR is 7.0 K when the urbanization rate is near 0.0, and 7.5 K when the urbanization rate is near 1.0 (Fig. 6c). The difference in the simulated DTR between the two (0.5 K) is smaller than that in the observed DTR (1.0 K) because NHRCM does not include the effects of urbanization.

The reduction in DTR in urban areas, compared with rural areas, is consistent with previous studies. For example, Gallo et al. (1996) investigated DTR at observation stations in the USA and evaluated the effects of land use/land cover changes. They found significant differences in the climatological DTR and attributed these differences predominantly to land use/land cover associated with the observation stations. Kalnay and Cai (2003) estimated the impact of urbanization by comparing trends in observed surface temperature in the USA and corresponding trends in global reanalysis data. Their results suggested that half of the observed decrease in DTR was due to urban and other land use changes. In China, Wang et al. (2012) used station observations to evaluate the urbanization effect on DTR and found that DTR decreased faster at urban than at rural stations. Furthermore, Brown and DeGaetano (2010) utilized differences in DTR between urban and rural areas for statistical discrimination between urban and rural climates. They found that DTR and nighttime dewpoint depression range indices provided the best classification

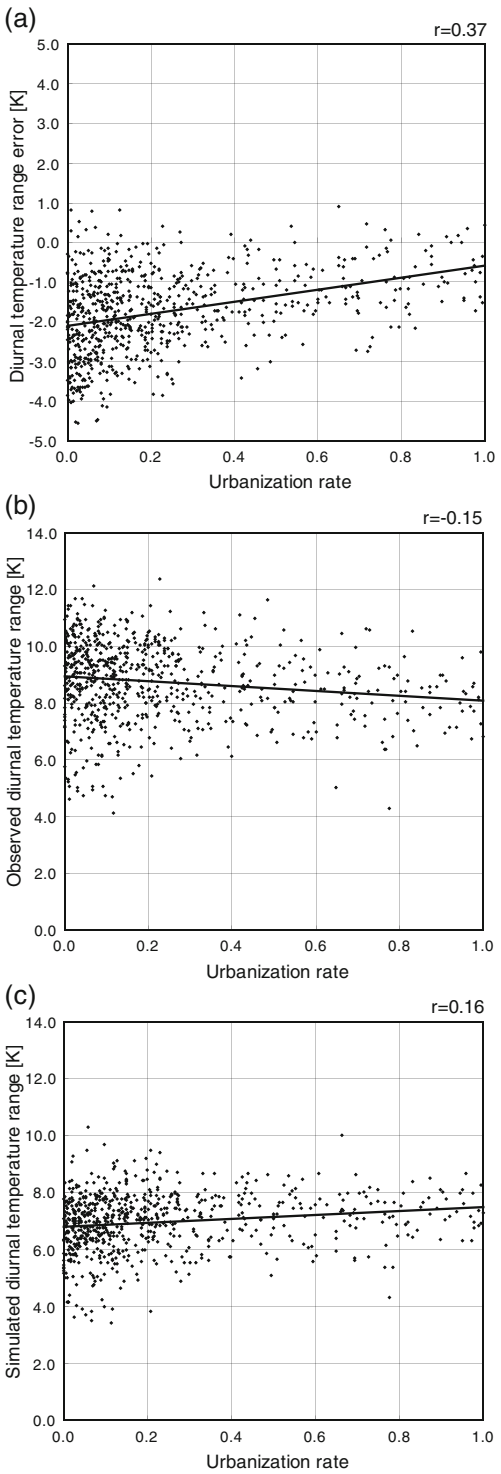

Fig. 6 Scatter diagram of the urbanization rate defined in the text. **a** DTR error, the difference in the annual average of DTR between NHRCM5 output and AMeDAS observation (model minus observed); **b** annual average of the observed DTR; and **c** annual average of the simulated DTR. The *regression line* and the correlation coefficient (*r*) between urbanization rate and temperature error are also indicated

variables, based on station data in the USA. This technique in cross-validation analysis correctly classified 93 % of the meteorological stations.

4.3 Temperature error in rural areas

NHRCM5 simulation produces biases in monthly mean temperatures, although the bias in the annual mean temperature is quite small. In rural areas where the urbanization rate is low, summertime biases in monthly mean temperature are positive, and wintertime biases are negative (Fig. 5). It is necessary to examine whether or not the simulated temperature in the free atmosphere, where the effects of the underlying ground are smaller, has biases in rural areas. Temperature fields in 850 hPa are, therefore, investigated in order to clarify this issue. The simulated temperature in 850 hPa is compared with that in the reanalysis data (JRA25) provided by JMA (Onogi et al. 2007). Monthly mean values averaged over the land areas of Japan are used for comparison between temperatures at 850 hPa obtained from the NHRCM5 simulation and JRA25 data, where only data with an urbanization rate of less than 0.2 are used.

Biases are detected in the simulated 850-hPa temperature as well as in the simulated surface air temperature. The biases are negative from September to the following April but are positive or nearly 0 for the rest of the year (Fig. 7). The wintertime negative bias and summertime positive or small bias correspond to those of surface air temperature. The time evolution of the bias is also in good agreement with that of surface air temperature, although the two values differ slightly from September to November. These results suggest that the biases in surface air temperature are due mainly to the large-scale temperature fields. How the simulated 850-hPa temperature is biased is an important question but is beyond the scope of this study.

The underestimation of the simulated DTR is relatively large in rural areas (Fig. 6). The simulated annual mean Tx is underestimated, and Tn is overestimated; however, the errors in Ta are relatively small when the urbanization rate is near 0 (Fig. 4). Figure 8 plots the time series of bias in monthly mean DTR averaged over the areas where the urbanization rate is less than 0.2. The DTR biases remain nearly constant (−2.0 K for all months). This result suggests that the causes of the biases are not in the large-scale atmospheric circulation but in the local-scale surface processes (e.g., sensible and latent heat fluxes from the land surface). It might be speculated that sensible heat fluxes are underestimated and/or latent heat fluxes are overestimated. However, it is difficult to verify this speculation because observations of the heat fluxes are generally unavailable.

The errors in Ta and DTR are responsible for those in Tx and Tn. Figure 9 plots the time series of bias in monthly mean Tx and Tn averaged over the areas where the urbanization rate is less than 0.2. Wintertime cold biases in Tx and nearly 0 biases in Tn are explained by cold biases in Ta and negative biases in DTR. In contrast, summertime warm biases in Tn and reduced cold biases in Tx are explained by warm biases in Ta and negative biases in DTR. It is important to keep in mind that the DTR biases remain nearly constant in time.

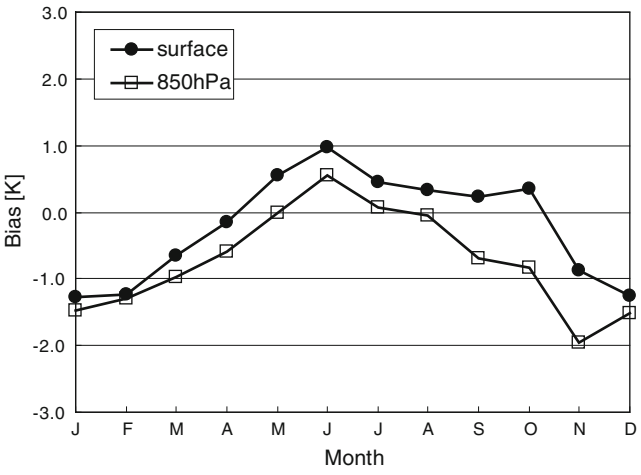

Fig. 7 Time series of bias in the monthly average of daily mean temperature at the surface and at the 850-hPa level. Bias is defined as the difference between NHRCM5 output and AMeDAS observation at the surface and as the difference between NHRCM5 output and reanalysis data (JRA25) at the 850-hPa level

5 Summary

The performance of a well-developed NHRCM with a spatial resolution of 5 km with respect to temperature in the present-day climate of Japan was evaluated, and UHI

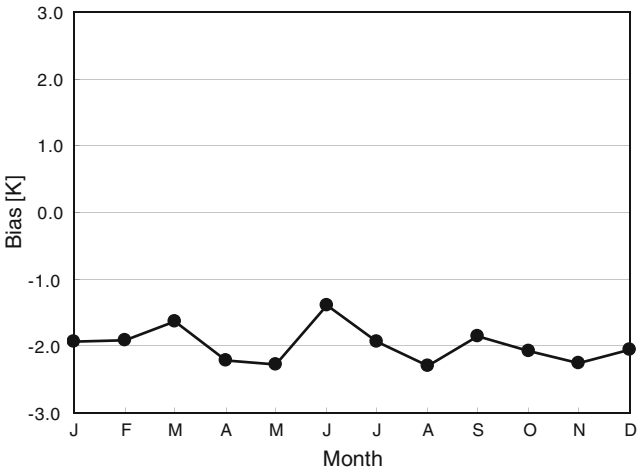

Fig. 8 Time series of bias in the monthly average of DTR at the surface. Bias is defined as the difference between NHRCM5 output and AMeDAS observation

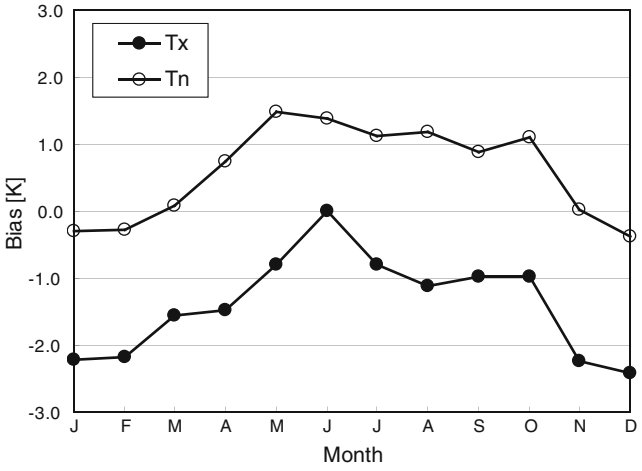

Fig. 9 Time series of bias in the monthly average of daily maximum and minimum temperatures. Bias is defined as the difference between NHRCM5 output and AMeDAS observation

intensity was estimated by comparing the model results and observations. The magnitudes of RMSE and bias for annual mean daily temperatures (Ta, Tx, and Tn) were within 1.5 K, demonstrating that the temperatures of the present-day climate were reproduced well by NHRCM. These small errors indicated that temperature variability produced by local-scale phenomena was represented well by the model with a higher spatial resolution. Also, the magnitudes of RMSE and bias in the annual mean Tx were relatively large compared with those in Ta and Tn.

In order to find reasons for the relatively large magnitudes of RMSE and bias in the annual mean Tx, the horizontal distributions of the error (defined as the difference between simulated and observed temperatures (simulated minus observed)) were examined. Negative error in the annual mean Tn was noticeable in three major metropolitan areas: Tokyo, Osaka, and Nagoya. These negative errors in urban areas seemed to affect the cold bias in Tx.

Therefore, the relationship between underestimation of temperature and degree of urbanization was examined quantitatively. To quantify the degree of urbanization, we used National Land Numerical Information provided by the Ministry of Land, Infrastructure, Transport, and Tourism. The degree of urbanization was defined as the urbanization rate of the areas within a grid area. Results indicated that the simulated Ta, Tx, and Tn were all underestimated in urban areas. Underestimations in urban areas were attributed to the treatment of urban areas in NHRCM, where the effects of urbanization (e.g., waste heat and artificial structures) were not included. In contrast, the simulated Tx was underestimated and Tn was overestimated in rural areas, although the errors in Ta were small, indicating that the simulated DTR was underestimated. Thus, the reason for the relatively large magnitudes of RMSE and bias in Tx was as follows. Tx errors were negative in both urban and rural areas, resulting in negative bias. In contrast, negative Tn errors in urban areas canceled several parts of positive errors in rural areas, reducing positive bias and making the bias close to 0. The bias in Ta was between those of Tx and Tn.

UHI intensity in Japan can be estimated statistically using the error discussed above. An index to evaluate statistical UHI intensity was defined as the difference in error between urban and rural areas. The index for Tn was larger than that for Tx, indicating that UHI intensity was more easily detected in nighttime than in daytime, consistent with previous studies where UHI intensity was generally stronger in nighttime than in daytime. The Ta index lay between those for Tx and Tn. Also, the index was larger in winter than in summer, indicating that UHI intensity was relatively strong during the warm seasons. These results demonstrated that UHI intensity over an area could be estimated by comparing the model results and observational data. The model results were not influenced by UHI effects because the effects of urbanization were not included in the model. The observational data, however, were directly affected by UHI. This difference was the key factor for detecting the effects of UHI.

Acknowledgments Numerical simulations using AGCM20 were conducted under the framework of the "Projection of the change in future weather extremes using super-high-resolution atmospheric models" supported by the KAKUSHIN Program of the Ministry of Education, Culture, Sports, Science, and Technology (MEXT) of Japan. These simulations were performed on the Earth Simulator.

References

Arnfield AJ (2003) Two decades of urban climate research: a review of turbulence, exchanges of energy and water, and the urban heat island. Int J Climatol 23:1–26. doi:10.1002/joc.859

Arritt RW, Rummukainen M (2011) Challenges in regional-scale climate modeling. Bull Amer Meteor Soc 92:365–368. doi:10.1175/2010BAMS2971.1

Beljaars ACM, Holtslag AAM (1991) Flux parameterization over land surfaces for atmospheric models. J Appl Meteor 30:327–341

Bourke RH, Garrett RP (1987) Sea ice thickness distribution in the Arctic Ocean. Cold Regions Sci and Tech 13:259–280. doi:10.1016/0165-232X(87)90007-3

Brown PJ, DeGaetano AT (2010) Using a discriminant analysis to classify urban and rural climate stations based on diurnal range of temperature and dewpoint depression. J Appl Meteor Climatol 49:2366–2379

Fujibe F (2011) Urban warming in Japanese cities and its relation to climate change monitoring. Int J Climatol 31:162–173. doi:10.1002/joc.2142

Gallo KP, Easterling DR, Peterson TC (1996) The influence of land use/land cover on climatological values of the diurnal temperature range. J Climate 9:2941–2944

Grimmond CSB (2006) Progress in measuring and observing the urban atmosphere. Theor Appl Climatol 84:3–22. doi:10.1007/s00704-005-0140-5

Hirai M, Ohizumi M (2004) Development of a new land-surface model for JMA-GSM. Extended abstract of 20th Conf Wea Anal. Forecasting/16th Conf NWP, P2.22. http://ams.confex.com/ams/84Annual/techprogram/paper_68652.htm. Accessed 1 Aug 2012

Ikawa M, Mizuno H, Matsuo T, Murakami M, Yamada Y, Saito K (1991) Numerical modeling of the convective snow cloud over the Sea of Japan: precipitation mechanism and sensitivity to ice crystal nucleation rates. J Meteor Soc Japan 69:641–667

IPCC (2007) Climate change 2007: the physical science basis. Contribution of Working Group I to the Fourth Assessment Report of the Intergovernmental Panel on Climate Change (Solomon S, Qin D, Manning M, Chen Z, Marquis M, Averyt KB, Tignor M, Miller HL (eds.)). Cambridge University, Cambridge, p 996

Kain JS (2004) The Kain–Fritsch convective parameterization: an update. J Appl Meteor 43:170–181

Kain JS, Fritsch JM (1990) A one-dimensional entrainment/detrainment plume model and its application in convective parameterization. J Atmos Sci 47:2784–2802

Kalnay E, Cai M (2003) Impact of urbanization and land-use change on climate. Nature 423:528–531

Kanada S, Nakano M, Hayashi S, Kato T, Nakamura M, Kurihara K (2008) Reproducibility of maximum daily precipitation amount over Japan by a high-resolution non-hydrostatic model. Sci Online Lett Atmos 4:105–108. doi:10.2151/sola.2008-027

Kanda M (2006) Progress in the scale modeling of urban climate: review. Theor Appl Climatol 84:23–33. doi:10.1007/s00704-005-0141-4

Kanda M (2007) Progress in urban meteorology: a review. J Meteor Soc Japan 85B:363–383

Kato T, Yamada Y, Nakano M (2010) Improvement of Kain–Fritsch convection parameterization scheme to suppress its false predictions of rainfall areas along coastal lines. CAS/JSC WGNE Res Act Atmos Ocean Model 40:4.07–4.08

Kida H, Koide T, Sasaki H, Chiba M (1991) A new approach to coupling a limited area model with a GCM for regional climate simulations. J Meteor Soc Japan 69:723–728

Kitagawa H (2000) Radiation processes. Separate Vol Annu Rep NPD 46:16–31 (in Japanese)

Kostopoulou E, Tolika K, Tegoulias I, Giannakopoulos C, Somot S, Anagnostopoulou C, Maheras P (2009) Evaluation of a regional climate model using in situ temperature observations over the Balkan Peninsula. Tellus 61A:357–370

Kurihara K, Ishihara K, Sasaki H, Fukuyama Y, Saitou H, Takayabu I, Murazaki K, Sato Y, Yukimoto S, Noda A (2005) Projection of climatic change over Japan due to global warming by high-resolution regional climate model in MRI. Sci Online Lett Atmos 1:97–100. doi:10.2151/sola.2005-026

Kusaka H (2008) Recent progress on urban climate study in Japan. Geograph Rev Japan 81:361–374

Landsberg HE (1981) The urban climate. Academic, New York

Lin YH, Farley RD, Orville HD (1983) Bulk parameterization of the snow field in a cloud model. J Clim Appl Meteor 22:1065–1092

Masson V (2006) Urban surface modeling and the meso-scale impact of cities. Theor Appl Climatol 84:35–45. doi:10.1007/s00704-005-0142-3

Mizuta R, Yoshimura H, Murakami H, Matsueda M, Endo H, Ose T, Kamiguchi K, Hosaka M, Sugi M, Yukimoto S, Kusunoki S, Kitoh A (2012) Climate simulations using the improved MRI-AGCM with 20-km grid. J Meteor Soc Japan 90A:233–258

Murakami M (1990) Numerical modeling of dynamical and microphysical evolution of an isolated convective cloud. The 19 July 1981 CCOPE cloud. J Meteor Soc Japan 68:107–128

Murakami M, Clark TL, Hall WD (1994) Numerical simulation of convective snow clouds over the Sea of Japan: two-dimensional simulation of mixed layer development and convective snow cloud formation. J Meteor Soc Japan 72:43–62

Murata A, Nakano M, Kanada S, Kurihara K, Sasaki H (2012) Summertime temperature extremes over Japan in the late 21st century projected by a high-resolution regional climate model. J Meteor Soc Japan 90A:101–122

Nakanishi M, Niino H (2004) An improved Mellor–Yamada level-3 model with condensation physics: its design and verification. Bound Layer Meteor 112:1–31

Nakano M, Kato T, Hayashi S, Kanada S, Yamada Y, Kurihara K (2012) Development of a 5-km-mesh cloud-system-resolving regional climate model at the Meteorological Research Institute. J Meteor Soc Japan 90A:339–350

Oke TR (1987) Boundary layer climates, 2nd edn. Methuen, London

Oke TR (2006) Towards better scientific communication in urban climate. Theor Appl Climatol 84:179–190. doi:10.1007/s00704-005-0153-0

Onogi K, Tsutsui J, Koide H, Sakamoto M, Kobayashi S, Hatsushika H, Matsumoto T, Yamazaki N, Kamahori H, Takahashi K, Kadokura S, Wada K, Kato K, Oyama R, Ose T, Mannoji N, Taira R (2007) The JRA-25 reanalysis. J Meteor Soc Japan 85:369–432. doi:10.2151/jmsj.85.369

Rayner NA, Parker DE, Horton EB, Folland CK, Alexander LV, Rowell DP, Kent EC, Kaplan A (2003) Global analyses of sea surface temperature, sea ice, and night marine air temperature since the late nineteenth century. J Geophys Res 108:D4407. doi:10.1029/2002JD002670

Rummukainen M (2010) State-of-the-art with regional climate models. WIREs Clim Chang 1:82–96. doi:10.1002/wcc.008

Saito K, Fujita T, Yamada Y, Ishida J, Kumagai Y, Aranami K, Ohmori S, Nagasawa R, Kumagai S, Muroi C, Kato T, Eito H, Yamazaki Y (2006) The operational JMA nonhydrostatic mesoscale model. Mon Wea Rev 134:1266–1298

Saito K, Ishida J, Aranami K, Hara T, Segawa T, Narita M, Honda Y (2007) Nonhydrostatic atmospheric models and operational development at JMA. J Meteor Soc Japan 85B:271–304

Sakakibara Y, Hara Y, Kato T (1996) The feature of heat island intensity with two extra stations method in the southeast part of Koshigaya City. Tenki 43:537–543 (in Japanese)

Sasaki H, Sato Y, Adachi K, Kida H (2000) Performance and evaluation of the MRI regional climate model with the spectral boundary coupling method. J Meteor Soc Japan 78:477–489

Sasaki H, Kurihara K, Takayabu I, Uchiyama T (2008) Preliminary experiments of reproducing the present climate using the non-hydrostatic regional climate model. Sci Online Lett Atmos 4:25–28. doi:10.2151/sola.2008-007

Sasaki H, Murata A, Hanafusa M, Oh'izumi M, Kurihara K (2011) Reproducibility of present climate in a non-hydrostatic regional climate model nested within an atmosphere general circulation model. Sci Online Lett Atmos 7:173–176. doi:10.2151/sola.2011-044

Urrutia R, Vuille M (2009) Climate change projections for the tropical Andes using a regional climate model: temperature and precipitation simulations for the end of the 21st century. J Geophys Res 114:D02108. doi:10.1029/2008JD011021

Wang K, Ye H, Chen F, Xiong Y, Wang C (2012) Urbanization effect on the diurnal temperature range: different roles under solar dimming and brightening. J Climate 25:1022–1027. doi:10.1175/JCLI-D-10-05030.1

Yabu S, Murai S, Kitagawa H (2005) Clear sky radiation scheme. Separate Vol Annu Rep NPD 51:53–64 (in Japanese)

Zhu J, Liang X-Z (2007) Regional climate model simulations of U.S. precipitation and surface air temperature during 1982–2002: interannual variation. J Climate 20:218–232